Functionally-Coupled Ion Channels Begin Co-assembling at the Start of Their Synthesis

Authors:

Roya Pournejati[1,2], Jessica M. Huang[1,2], Michael Ma[1,2], Claudia M. Moreno[2,3], Oscar Vivas[1,2*]

Affiliations:

[1] Department of Pharmacology, University of Washington

[2] Department of Neurobiology and Biophysics, University of Washington

[3] Howard Hughes Medical Institute

***Corresponding author:**

Oscar Vivas

Department of Pharmacology

Department of Neurobiology and Biophysics

University of Washington, School of Medicine

Box 357290

Seattle, WA 98195-7290

Email: vivas@uw.edu

Phone: (206) 543-0958

Summary

Calcium binding to BK channels lowers their activation threshold. Hence, BK channels are functionally coupled to calcium-permeable channels. This functional coupling requires proximity of two different types of channels. Formation of an ensemble at nanometer distances between BK and Ca_V1.3 channels exemplifies this unique organization. We investigated the mechanism underlying their structural organization, testing the hypothesis that the assembly between BK and Ca_V1.3 channels is formed before their insertion at the plasma membrane. Our design used four approaches: 1) to detect the interaction between BK and Ca_V1.3 proteins inside the cell, 2) to identify the membranes where intracellular ensembles reside, 3) to measure the proximity between their mRNAs, and 4) to look for protein interaction at the plasma membrane soon after the start of their translation. These measures showed that a percentage of transcripts for BK and Ca_V1.3 channels are close and that the newly synthesized proteins interact through the endoplasmic reticulum and Golgi. Comparisons were made with other proteins and transcripts, as well as with predictions of randomized localizations of BK channels. We found evidence of assembly between BK and Ca_V1.3 ensembles before their insertion at the plasma membrane.

Significant statement

This work explores the proximity between the mRNAs and between newly synthesized BK and Ca_V1.3 channels to discover that these channels get together early in their biogenesis. Experiments employed a heterologous expression system to study the steps of protein trafficking and an insulinoma cell line of pancreatic beta cells to study proximity of endogenous channel mRNAs. The results support a new paradigm for signaling complexes, proposing that their assembly is initiated already during protein synthesis and trafficking and before insertion at their final target destination in the plasma membrane.

Introduction

This work concerns the organization of functionally coupled voltage- and calcium-dependent potassium (BK) channels and voltage-gated calcium (Ca_V) channels.

BK channels (a.k.a. K_{Ca}1.1, Maxi-K, Slo1, KCNMA1) are named for their "big potassium (K^+)" conductance, since channel opening leads to unusually large, outward potassium currents and membrane repolarization. Their amino acid sequence is conserved throughout the animal kingdom from worms to mammals. BK channels are expressed in a wide variety of cell types, predominantly excitable cells but also non-excitable salivary, bone and kidney cells, making this channel responsible for a large range of physiological processes [1-9]. Phenotypes of pathological BK mutations in human patients are most prominent in the brain and muscle, and often manifest with seizures, movement disorders, developmental delay, and intellectual disability [10, 11]. BK is also implicated in other organ system functions, including but not limited to heart pace making, reproduction, and pancreatic glucose homeostasis[11, 12].

Since BK channels affect function in numerous physiological systems, their channel opening is meticulously regulated at the cellular level. BK is a voltage-gated channel, activated by membrane depolarization. Interestingly, BK has an additional gating mechanism that differentiates it from typical voltage-gated potassium channels; BK opening is gated by both voltage and intracellular calcium binding to a cytosolic regulatory domain. At the cytoplasmic resting free calcium concentration (~0.1 μM), BK channels remain closed [13]. However, the probability of opening increases both when the membrane potential depolarizes and when the local free calcium rises. Yet, increases of calcium are tightly confined by endogenous proteins that bind calcium with high affinity and extrusion mechanisms that take calcium inside organelles or outside the cell. Hence, BK activation relies on strategies to overcome these barriers. They bind calcium delimited to the point of entry at calcium channels.

In excitable cells, BK forms nanodomains with calcium channels that provide exclusive, localized supplies of intracellular calcium. Several subtypes of calcium channels form functional signaling complexes with BK, shifting BK activation voltages to more negative potentials [14-16]. One of these channels, Ca_V1.3 (a.k.a. *CACNA1D*), is unique in its electrophysiological profile as an L-type calcium channel, activating with fast kinetics at voltages as negative as -55 mV [17].

Ca_V1.3 is expressed in many of the same cell types as BK and is often functionally coupled with BK channels, enabling them to activate at more negative voltages. Notably, super-resolution microscopy shows that Ca_V1.3 organizes spatially into nanodomains near BK in the plasma membrane [15]. However, the mechanisms behind the assembly of BK and Ca_V1.3 complexes are unknown.

Several mechanisms for bringing ion channels together have been suggested (table 1). One proposes that it precedes protein insertion into the plasma membrane [18-20]. This mechanism has been observed in studies of hetero-multimers and even channels permeating different ions. The formation of these groups of proteins would start from their synthesis; possibly, even their mRNA transcripts are colocalized prior to translation. We explored this mechanism in relation to BK and Ca_V1.3 functional coupling. Here, we started by asking when BK and Ca_V1.3 channels cluster in the cell. We looked for BK and Ca_V1.3 ensembles at intracellular membranes of the ER, at ER exit sites, and at the Golgi. We also investigated the proximity between mRNA transcripts of BK and Ca_V1.3.

Definitions used in this manuscript

To guide the reader and prevent confusion on the terms used, we introduce the following nomenclature, which is also illustrated in Figure 1. Molecular complex: an array of several polypeptides with a defined function. In our case, a BK channel is a molecular complex of four alpha subunits whose function is to permeate ions, also referred as a homo-tetramer. Cluster: we define a cluster as the accumulation of proteins. In our work, cluster refers to an

Mechanism	Description	Source
Co-translation of heteromeric channel subunits	mRNA transcripts and nascent proteins of hERG heteromeric subunits form molecular complexes during protein translation.	[18]
Co-translation of channels permeating different ions	Potassium channel hERG and sodium channel SCN5A form complexes of mRNA transcripts and nascent proteins during protein translation.	[19]
Membrane curvature sensing	Clusters of Piezo1 channels enriches in membrane invaginations.	[21]
ER membrane protein complex	ER membrane complex acts as a chaperone for heteromeric channel assembly.	[22]
Scaffolding proteins	Scaffolding protein AKAP150 is required for abnormal gating of Ca_V1.2-LQT8 channels.	[23]
Random insertion	Clusters of Ca_V1.2, Ca_V1.3, BK, and TRPV4 are proposed to be randomly formed into the plasma membranes of smooth muscle, cardiac muscle, hippocampal neurons, and tsA-201 cells.	[23]

Table 1. List of mechanisms described for the interaction between channel subunits, channels of the same type (clusters), or ensembles of channel families permeating different ions.

accumulation of BK channels or an accumulation of calcium channels. In a previous manuscript, we also referred to these as homo-clusters. Ensemble: we define ensemble as the collection of different types of proteins that facilitate functional coupling and compartmentalization of a signaling complex. These proteins can also be in clusters; in such cases, an ensemble is the aggregation of clusters. In the present work, ensemble refers to a coordinated collection of BK and Ca_V channels. It is also used to refer to the assembly of BK clusters with Ca_V clusters. In a previous manuscript, we referred to this as hetero-clusters.

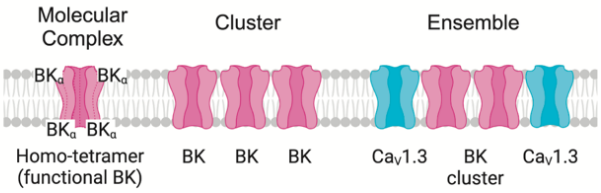

Figure 1. Representation of molecular complex, cluster, and ensemble.

Materials and Methods

Cell culture:

We used tsA-201 cells to co-express BK and Ca_V1.3 channels heterologously. Cells were grown in DMEM (Gibco) supplemented with 10% fetal bovine serum and 0.2% penicillin/streptomycin. We used rat insulinoma (INS-1) cells to study endogenous levels of transcripts and proteins of the channels. INS-1 cells were cultured in RPMI high glutamate medium (Gibco) with 10% fetal bovine serum, 0.2% penicillin/streptomycin, 10 mM HEPES (Gibco), 1 mM sodium pyruvate (Gibco), and 50 μM 2-mercaptoethanol. Both cell types were passaged twice a week and incubated in 5% CO_2 at 37°C.

Plasmids and transfection:

Cells were transfected with 0.1– 0.4 μg DNA per plasmid, plated for 24 hours on poly-D-Lysine coated coverslips, and used for experiments. Lipofectamine 3000 (Invitrogen, RRID: L30000) was used for the transfection. DNA clones of Ca_V1.3, BK channels, PH-PLCδ GFP, ER moxGFP, pmGFP-Sec16S and Golgi-mGFP were obtained from Addgene (RRID:SCR_002037). Auxiliary subunits for Ca_V1.3 channels, Ca_Vβ3 and Ca_Vα2δ1 (from Diane Lipscombe, Brown University, RI), were transfected as well. No BK channel auxiliary subunits were transfected.

Antibodies:

Ca_V1.3 channels were immuno-detected with a rabbit primary antibody recognizing residues 809 to 825 located at the intracellular II-III loop of the channel (DNKVTIDDYQEEAEDKD), kindly provided by Drs. William Catterall and Ruth Westenbroek [25]. BK channels were detected using the anti-Slo1 mouse monoclonal antibody clone L6/60. The goat

polyclonal GFP antibody was against the recombinant full-length protein corresponding to *Aequorea victoria* GFP. Anti-58K Golgi protein antibody was used to mark the Golgi. Specificity of antibodies was tested in un-transfected tsA-201 cells (Figure 1- supplementary 1). The secondary antibodies tagged with Alexa dyes were Donkey anti-mouse Alexa-647, Donkey anti-rabbit Alexa-555, Donkey anti-goat Alexa-488, all from Molecular Probes.

Immunostaining:

Cells were fixed with freshly prepared 4% paraformaldehyde for 10 min. After washing, aldehydes were reduced with 0.1% $NaBH_4$ for 5 minutes at 21˚C and then washed again. Nonspecific binding was blocked with 3% bovine serum albumin (Thermo Scientific). Cells were permeabilized with 0.25% v/v Triton X-100 in PBS for 1 hour. Primary antibodies were used at 10 µg/ml in blocking solution and incubated overnight at 4°C. After washing, secondary antibodies at 2 µg/ml were incubated for 1 hour at 21˚C. For single-molecule localization microscopy, fixed and stained cells were imaged in GLOX imaging buffer containing 10 mM β-mercaptoethylamine (MEA), 0.56 mg/ml glucose oxidase, 34 µg/ml catalase, and 10% w/v glucose in Tris-HCl buffer. Washing steps indicated in all the methods in this paper include 3 cycles of rinses and rocking for 5 minutes with PBS. Cells were imaged using an inverted AiryScan microscope or an ONI Nanoimager with super-resolution capabilities.

Proximity ligation assay (PLA):

Cells were fixed with freshly prepared 4% paraformaldehyde for 10 minutes. After washing, aldehydes were reduced with 50 mM glycine for 15 minutes at 21˚C. After another round of washes, PLA was performed according to manufacturer instructions (Duolink® In Situ Red Starter Kit). Cells were blocked and permeabilized with Duolink blocking solution. Primary antibodies were used at 10 µg/ml in Duolink antibody diluent and incubated overnight at 4°C. The Duolink® In Situ PLA® probe anti-rabbit PLUS and anti-mouse MINUS were used as secondary antibodies, followed by ligation and amplification. For PLA combined with immunostaining, PLA was followed by a secondary antibody incubation with Alexa Fluor-488 (Molecular Probes) at 2 µg/ml for 1 hour at 21˚C. Coverslips were mounted using ProLong™ Gold Antifade Mountant with DAPI. Cells were imaged using an inverted Zeiss AiryScan microscope.

Single molecule In Situ Hybridization (RNASCOPE):

Manual RNAscope assay was performed using RNAscope™ Multiplex Fluorescent V2 Assay according to the

manufacturer's protocol. The RNAScope assay consists of target probes and a signal amplification system composed of a preamplifier, amplifier, and label probe. A schematic RNAscope assay procedure is shown in Figure 4- Supplementary 1. Briefly, Cells were fixed with 4% paraformaldehyde for 30 minutes, washed, dehydrated, and then rehydrated with ethanol, and permeabilized with 0.1% Tween-20 in PBS. Next, cells were quenched with H_2O_2 and treated with Protease III. Probes were hybridized for 2 hours at 40°C followed by RNAscope amplification and then fluorescent detection. Coverslips were mounted using ProLong™ Gold Antifade Mountant with DAPI. We used the following RNAscope probes: RNAscope 3-plex Positive Control Probes, RNAscope 3-plex negative control probes, RNAscope™ Probe- Rn-Ryr, RNAscope™ Probe- Rn-Scn9a, RNAscope Probe- Rn-Kcnma1-C3, RNAscope Probe- Rn-Cacna1d-C2 and RNAscope Probe- Rn-Gapdh. Cells were imaged on the inverted AiryScan microscope.

High resolution imaging:

Cells were imaged using an inverted AiryScan microscope (Zeiss LSM 880) run by Zen black v2.3 software and equipped with a plan apochromat 63X oil immersion objective with 1.4 NA. Fluorescent dyes were excited with a 405 nm diode, 458–514 nm argon, 561 nm, or 633 nm laser. Emission light was detected using an Airyscan 32 GaAsP detector and appropriate emission filter sets. The point spread functions were calculated using Zen black software and 0.1 µm fluorescent microspheres. The temperature inside the microscope housing was 22°C. Images were analyzed using ImageJ (NIH).

Super resolution imaging:

Direct stochastic optical reconstruction microscopy (dSTORM) images of BK and Ca_V1.3 overexpressed in tSA-201 cells were obtained using ONI Nanoimager microscope equipped with a 100X oil immersion objective with a 1.4 NA, an XYZ closed-loop piezo 736 stage, and triple emission channels split at 488, 555 and 640 nm. Samples were imaged in GLOX imaging buffer at 35°C. The acquired single-molecule data were filtered using NImOS software (v.1.18.3, ONI) and further processed in ImageJ (NIH).

Image Scrambling

Images were binarized as .tif images, and their respective cell perimeter coordinates were exported as .csv files by ImageJ (NIH). Processed binary images were then analyzed by our SpotScrambler (https://github.com/jehuang2/SpotScramble) Python program. SpotScrambler first extracts the areas of fluorescent particles in

the binary image. SpotScrambler then redraws the fluorescent particles as circles at randomized coordinates within cell perimeter boundaries. SpotScrambler accurately preserves particle number and particle sizes, averaging less than 1% difference in total area of fluorescent particles between pre-SpotScrambler and post-SpotScrambler images. To ensure reliable randomization for each experiment, results were averaged between 3 trials of SpotScrambler.

Data analysis

Excel (Microsoft), and Prism (GraphPad) were used to analyze data. ImageJ was used to process images. For PLA and RNAScope experiments we used custom-made macros written in ImageJ. Localization maps acquired from super-resolution experiments were reconstructed using NImOS software. Processing consisted of thresholding and binarization of images to isolate labeled structures. Particles were analyzed to calculate both the area and number of particles and the colocalization from these images. Processing of data from PLA experiments included background subtraction. One-way ANOVA and non-parametric statistical test (Mann-Whitney Wilcoxon) were used to test for statistical significance. p-values <0.05 were deemed statistically significant. The number of cells used for each experiment is detailed in each figure legend.

Results

BK and Ca_v1.3 ensembles are found inside the cell

BK and Ca_V ensembles have been observed at the plasma membrane [14-16]. However, a clear understanding of when or how BK and Ca_V complexes assemble is missing. A simple mechanism supposes that these ensembles organize only at the plasma membrane. Here, we tested an alternative hypothesis that BK and Ca_V assemble inside the cell (Figure 2A). To test this idea, we used proximity ligation assay (PLA) and antibodies against BK and Ca_V1.3 channels. Only when these antibodies are closer than 40 nm, can ligation and amplification occur, resulting in the formation of fluorescent puncta (Figure 2B), here referred to as PLA puncta. Hence, the PLA puncta in Figure 2C represent BK and Ca_V1.3 ensembles. We first analyzed Z-projections, in which all the puncta in the cell volume are added, and found a density of 5.8 ± 1.0 / 10 μm^2. In a different experiment, we analyzed the puncta density for each focal plane of the cell and compared the puncta at the plasma membrane to the rest of the cell. We visualized the plasma membrane with a biological sensor tagged with GFP (PH-PLCδ-GFP) and probed against GFP using an antibody (Figure 2E). We identified clear puncta at the plasma membrane, but to our

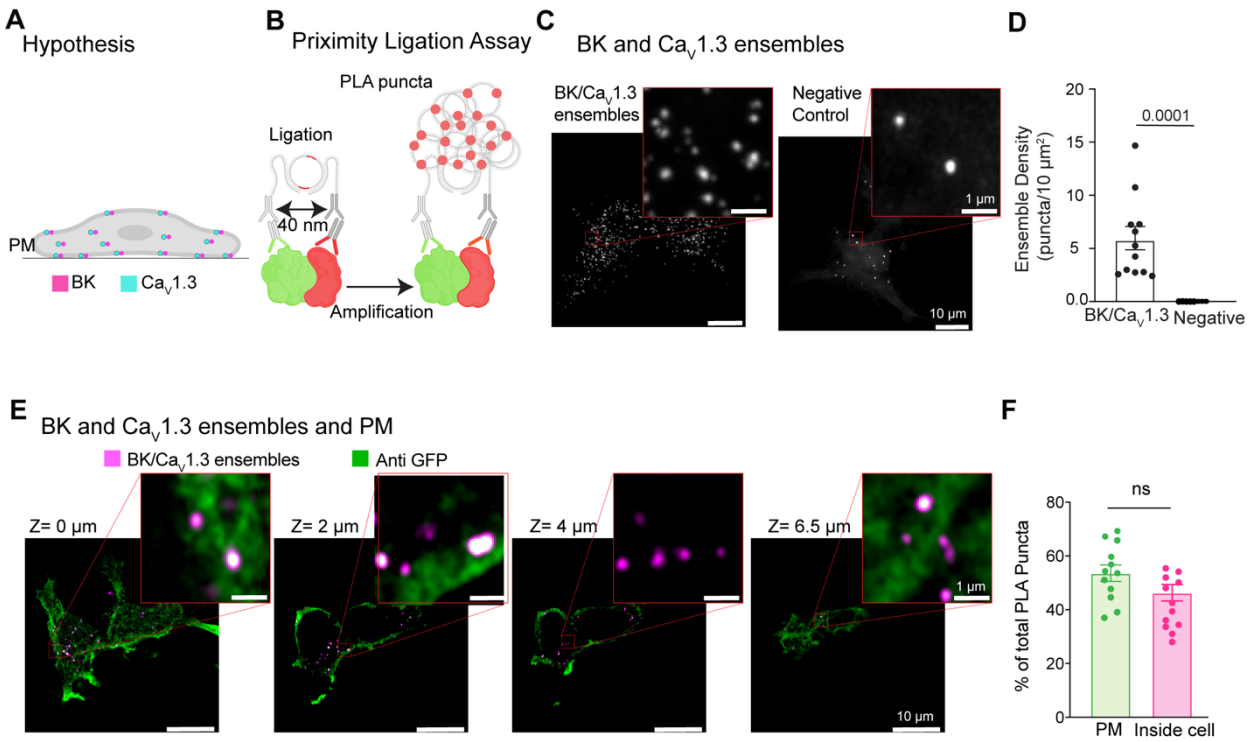

Figure 2. BK and Ca$_V$1.3 ensembles are found inside the cell. A. Diagram of the hypothesis: Ensembles of BK (magenta) and Ca$_V$1.3 (cyan) are on intracellular membranes and on the plasma membrane. **B.** Illustration of the technique to detect BK and Ca$_V$1.3 ensembles. Proximity ligation assay is used to detect the ensembles. **C.** Confocal images of fluorescent puncta from PLA experiments in tsA-201 cells. Left: Cells were transfected and probed for BK and Ca$_V$1.3 channels. Right: negative control. Cells were transfected and probed only for BK channels. Enlargement of a selected region is shown in the inset. **D.** Scatter dot plot comparing puncta density of ensembles of BK and Ca$_V$1.3 to the negative control. Data points are from n = 12 cells from BK and Ca$_V$1.3 clusters and from n = 14 cells from negative control. *p*-values are shown at the top of the graphs. **E.** Confocal images of fluorescent PLA puncta at different focal planes co-labeled against GFP at the plasma membrane. Cells were transfected with BK, Ca$_V$1.3, and PH-PLCδ-GFP and probed for BK and Ca$_V$1.3 channels and GFP. The plane of the PM was set as zero in the Z axis. PLA puncta are shown in magenta, and the plasma membrane in green. Distance from the PM plane is labeled with the Z values on top of each image. Enlargements of the same region in Z are shown in the insets. **F.** Scatter dot plot comparing BK and Ca$_V$1.3 cluster abundance at PM and inside the cell. Data points are from n = 12 cells. Scale bar is 10 µm and 1 µm in the insets.

surprise, also puncta inside the cell. We found that 46 ± 3 % of the puncta were localized on intracellular membranes, whereas 54 ± 3 % were at the plasma membrane. This finding is consistent with our supposition that BK and Ca$_V$1.3 channels get together at membranes inside the cell.

BK and Ca$_V$1.3 ensembles localize at ER and ER exit sites.

We next investigated the identity of the intracellular membranes where these PLA puncta were found. A large component of the intracellular membranes is the endoplasmic reticulum (ER), where channels are inserted after translation. To determine whether BK and Ca$_V$ associate in the ER (Figure 3A), we combined PLA with immunodetection. As before, PLA probed for ensemble formation between BK and Ca$_V$ channels, whereas a KDEL-moxGFP label

identified the ER (Figure 3B). To avoid disruption of organelle architecture, we used the monomeric mox version of KDEL-GFP, which is optimized to reduce oligomerization in the ER environment [26]. Neither overexpression of KDEL-moxGFP nor fixation altered the ER structure as the tubule width remained around 150 nm for either condition (Figure 3C), a value in agreement with the literature [27, 28]. To assess the percentage of PLA puncta co-localizing with the ER, we employed two different cell lines, our overexpression system (tsA-201 cells) and a rat insulinoma cell line (INS-1) that expresses BK and Ca$_V$1.3 channels endogenously. In this and following experiments, we analyze one focal plane, in the middle of the cell, to quantify PLA puncta

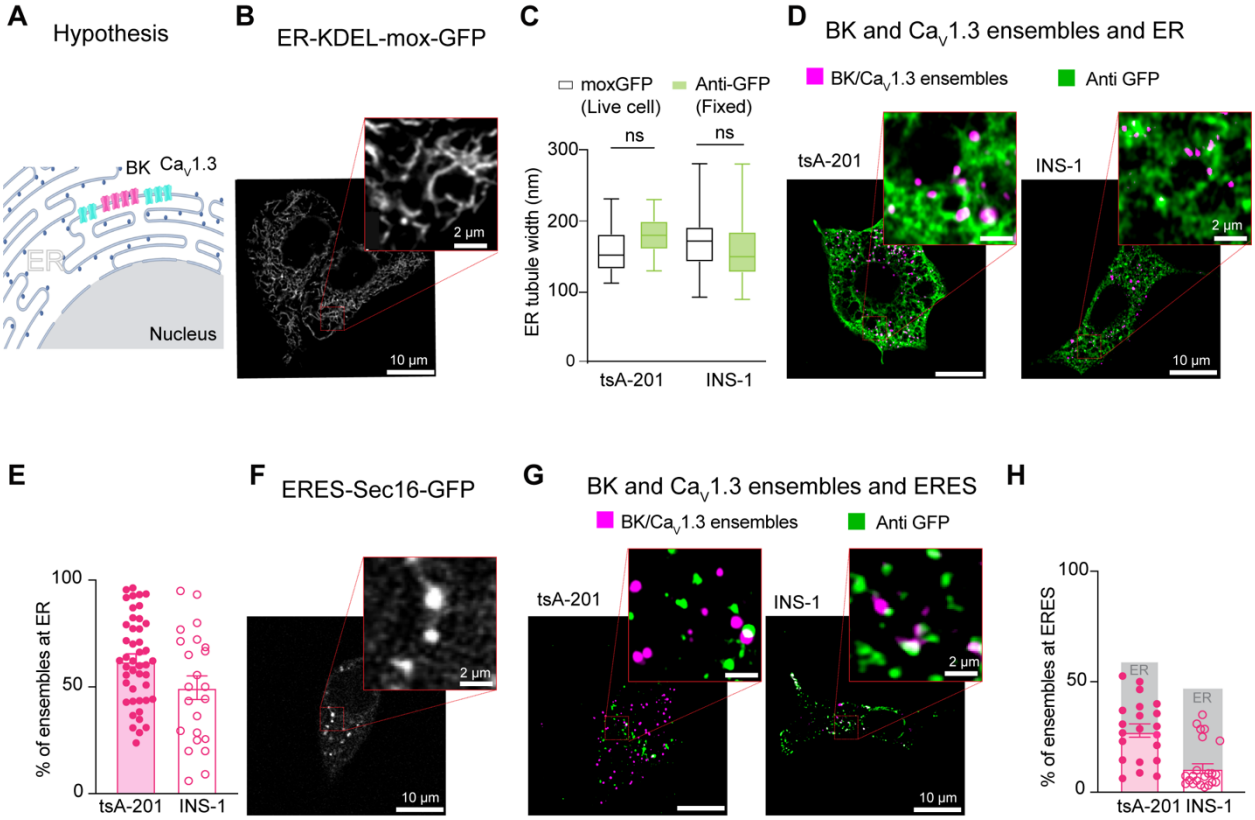

Figure 3. BK and Ca$_V$1.3 ensembles localize at ER and ER exit sites (ERES). A. Diagram of the hypothesis: Ensembles of BK (magenta) and Ca$_V$1.3 (cyan) can be found at the ER membrane. **B.** Representative image of the ER labeled with exogenous GFP in INS-1 cells. Cells were transfected with KDEL-moxGFP. Enlargement of a selected region is shown in the inset. **C.** Comparison of the ER tubule distance in live and fixed tsA-201 and INS-1 cells. Data points are from n = 23 tsA-201 cells, n = 27 INS-1 cells **D.** Confocal images of PLA puncta (magenta) and ER (green) in tsA-201 (left) and INS-1 (right) cells. Cells were transfected with BK, Ca$_V$1.3, and KDEL-moxGFP. PLA puncta reveal ensembles of BK and Ca$_V$1.3. ER is shown in green. **E.** Comparison of BK and Ca$_V$1.3 ensembles found at the ER and relative to all PLA puncta in the cell. Values are given in percentages. **F.** Representative image of ER exit sites labeled with sec16-GFP. Magnification is shown in the inset. **G.** Thresholded images of PLA puncta and ER exit sites. Left and right are the same as in D, but cells were transfected with Sec16-GFP instead of KDEL. **H.** Percentage of BK and Ca$_V$1.3 ensembles found at ER exit sites relative to all PLA puncta. Grey bars show the percentage of ensembles found in the ER. Data points are from n = 45 tsA-201 cells for ER; n = 21 tsA-201 cells for ERES; n = 23 INS-1 cells for ER; n = 23 INS-1 cells for ER exit sites. Scale bar is 10 µm and 2 µm in the magnifications.

colocalization with ER membrane. Figure 3D shows PLA puncta in the same space as the ER. Comparing the overexpression and endogenous systems, 63 ± 3% versus 50 ± 6% of PLA puncta were localized at the ER (Figure 3E). To rule out the possibility that the colocalization between ensembles and ER is caused by the fact that the ER labeling occupies a large area of the cell, we labeled the ER exit sites with Sec16-GFP and probed for BK and Ca_V1.3 ensembles with PLA (Figure 3F). We found 28 ± 3% of BK and Ca_V1.3 ensembles colocalized at ER exit sites in tsA-201 cells, and 11 ± 2% in INS-1 cells (Figure 3G). Although the percentage of colocalization between ensembles and the ER or the ER exit sites cannot be compared or used to understand the dynamics of the ensembles, these results support the conclusion that ensembles are localized in the ER, and suggest that BK and Ca_V1.3 channels traffic together through the ER and exit together.

BK and Ca_V1.3 ensembles go through the Golgi.

Channels are modified in the Golgi after synthesis (Figure 4A), so we asked whether PLA puncta formed by BK and Ca_V1.3 ensembles are found in the Golgi. Using the same strategy, we labeled Golgi with Gal-T-mEGFP (Figure 4B) and detected BK and Ca_V ensembles using PLA. To confirm that the overexpressed Gal-T-mEGFP labels the Golgi specifically without altering its structure, we compared the region detected using the antibody against GFP to the region detected using a primary antibody against the Golgi protein 58K (Figure 4C). 58K is a Golgi specific peripheral protein that localizes at the cytosolic face of Golgi [29]. The overlay shows that the GFP signal labels the same region as the antibody against 58K. When assessing the presence of BK and Ca_V1.3 clusters in the Golgi, we found that 31 ± 5% of PLA puncta were localized at the Golgi in the overexpression system and 25 ± 4% in the endogenous cell model (Figure 4E).

We performed controls to confirm that the formation of ensembles between the two channels was not coincidental but rather the result of structural coupling. We tested the formation of PLA puncta between BK channels and the Golgi protein 58K. We also tested for Ca_V1.3 and 58K. We did not find PLA puncta when the proximity between the channels and 58K was probed (Figure 4F), supporting the idea that PLA puncta between BK and Ca_V1.3 channels found at the Golgi represent specific coupling.

It is important to clarify that the percentages provided in this work cannot be added up to understand the distribution of ensembles along the biosynthetic pathway of the channels. The percentage in each

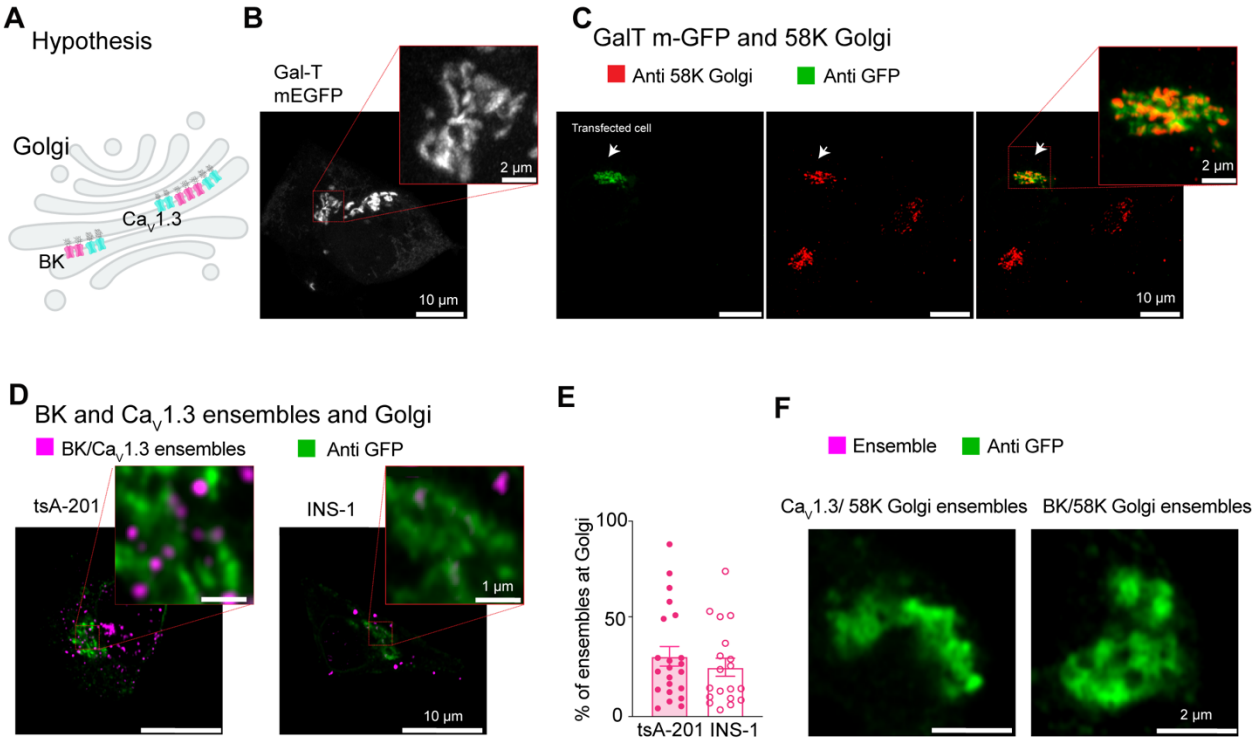

Figure 4. BK and Ca$_V$1.3 ensembles go through the Golgi. A. Diagram of the hypothesis: PLA puncta detecting ensembles between BK (magenta) and Ca$_V$1.3 (cyan) channels can be found at the Golgi membrane. **B.** Representative confocal image of the Golgi structure with exogenous GFP in INS-1 cells. Cells were transfected with Gal-T-mEGFP. Enlargement is shown in the inset. **C.** Representative images of fixed cells co-stained with antibodies against Gal-T-mEGFP (left) in green and 58K-Golgi (middle) in red. Overlay (right). **D.** Representative confocal images of PLA puncta and Golgi. TsA-201 cells were transfected with BK, Ca$_V$1.3 and Gal-T-mEGFP (left), and INS-1 cells were transfected only with Gal-T-mEGFP (right). PLA puncta are shown in magenta. Golgi is shown in green. **E.** Scatter dot plot of percentage of BK and Ca$_V$1.3 ensembles found at the Golgi relative to all PLA puncta in tsA-201 and INS1 cells. Data points are from n = 22 tsA-201 cells and n = 19 INS-1 cells. **F.** Representative image of PLA puncta and Golgi. tsA-201 cells were transfected with BK, Ca$_V$1.3 and Gal-T-mEGFP. Left: PLA was done against BK and 58K Golgi (magenta) and Golgi is shown in green. Right: PLA was done against Ca$_V$1.3 and 58K Golgi (magenta) and Golgi is shown in green. Scale bars: 10 µm and 2 µm in panels B and C; 10 µm and 1 µm in panel D; 2 µm in panel F.

membrane compartment was compared to the total percentage of ensembles observed in each cell for that particular experiment. Therefore, there is expected overlap between our measurements due to i) optical resolution and ii) the effect of not comparing all the organelles in the same cell. Considering these limitations, we interpreted our results as follows: about one half of the ensembles are found inside the cell. The other half corresponds to ensembles at the plasma membrane. From the half inside the cell, roughly one third of ensembles are found in the Golgi, and another third in ER exit sites. The remaining percentage of ensembles are found in other regions of the

ER and membranes that we did not measure, such as vesicles.

BK mRNA and Ca_V1.3 mRNA co-localize.

How is it that BK and Ca_V1.3 proteins come in close proximity in membranes of the ER, ER exit sites and the Golgi? To explore the origins of the initial association, we hypothesized that the two proteins are translated near each other, which could be detected as the colocalization of their mRNAs (Figure 5A and B). The experiment was designed to detect single mRNA molecules from INS-1 cells in culture. We performed multiplex in-situ hybridization experiments using the RNAscope fluorescence detection kit to be able to image three mRNAs simultaneously in the same cell and acquired the images in a confocal microscope with high resolution. Supplementary Figure 4.1 shows images completely void of fluorescent signal from INS-1 cells probed for bacterial mRNA (negative control, Figure S5.1A) and images of INS-1 cells probed for mammalian mRNAs expected to be in these cells (positive control, Figure S5.1B). The probes against the mRNAs of interest and tested in this work were designed by Advanced Cell Diagnostics. We confirmed the specificity of the probes by performing in situ hybridization against BK mRNA (*KCNMA1*), Ca_V1.3 mRNA (*CACNA1D*), type 2 ryanodine receptors mRNA (*RyR2*), and Na_V1.7 mRNA (*SCN9A*) in non-transfected cell lines (Figure S5.1C and D).

Probes against *GAPDH* mRNA were used as a control in the same cells using the multiplex capability of this design. Transcripts were detected at different expression levels. *GAPDH* and *CACNA1D* mRNAs were more abundant (134 and 33 mRNA/100 μm^2, respectively) than *KCNMA1* mRNA (12 mRNA/100 μm^2, Figure 5C). Interestingly, the abundance of *KCNMA1* transcripts correlated more with the abundance of *CACNA1D* transcripts than with the abundance of *GAPDH*, a standard housekeeping gene (Figure 5D and E). Furthermore, *KCNMA1* and *CACNA1D* mRNA colocalized by 60 ± 4%, which was 20% more than with *GAPDH* mRNA (Figure 4F). To rule out the potential influence of difference in mRNA abundance, we assessed *CACNA1D* mRNA colocalization with randomized, computer-generated *KCNMA1* mRNA signals. We found that colocalization between randomized *KCNMA1* mRNA and genuine *CACNA1D* mRNA was also 20% less than the colocalization of genuine *KCNMA1* mRNA and genuine *CACNA1D* mRNA. These results suggest that some fraction of mRNAs for *KCNMA1* and *CACNA1D* channels are translated nearby, so the channel proteins potentially could be inserted into the same regions of the ER. We suggest that the newly

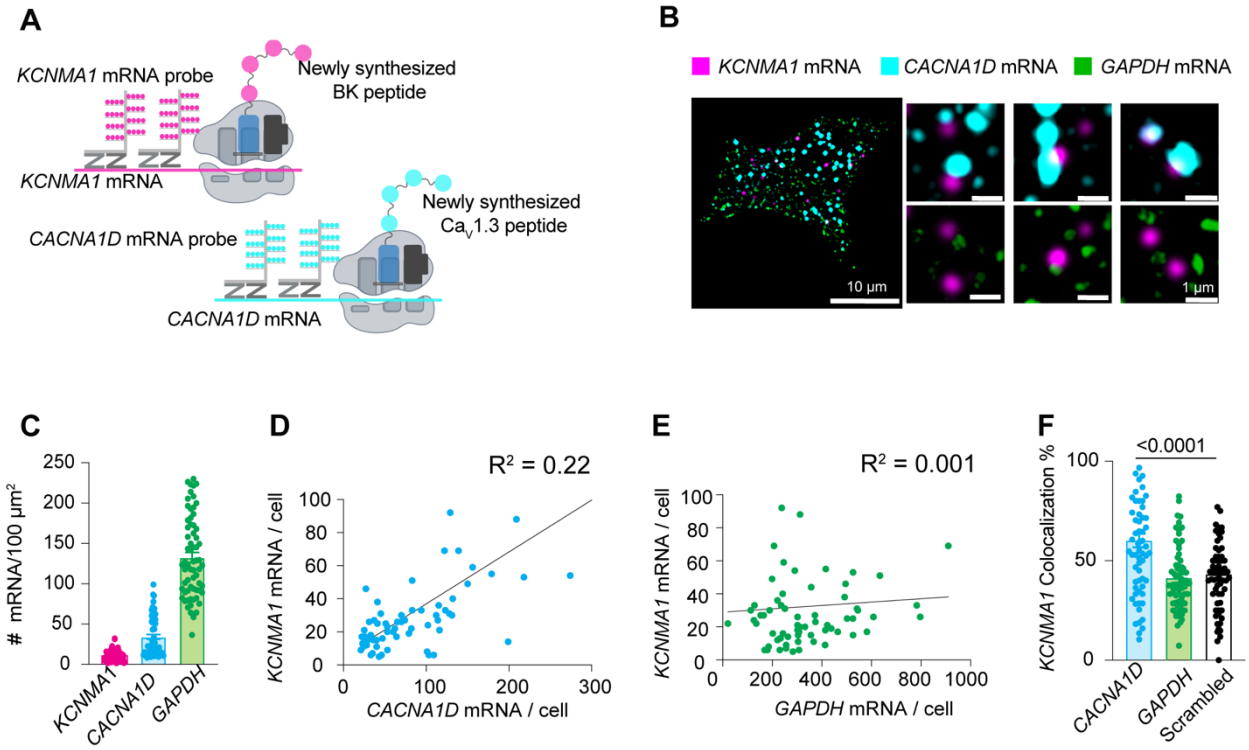

Figure 5. BK mRNA (*KCNMA1*), Ca$_V$1.3 mRNA (*CACNA1D*) co-localize. A. Diagram of the hypothesis: *KCNMA1* and *CACNA1D* mRNAs are found in close proximity to be translated in the same neighborhood. **B.** Images of fluorescent puncta from RNA scope experiments showing *KCNMA1* mRNA in magenta *CACNA1D* mRNA in cyan, and *GAPDH* mRNA in green. Right, magnification of three ROI. **C.** Comparison of mRNA density of *KCNMA1*, *CACNA1D*, and *GAPDH*. **D.** Correlation plot of mRNA abundance of *KCNMA1* and *CACNA1D* per cell. **E.** Correlation plot of mRNA abundance of *KCNMA1* and *GAPDH* per cell. **F.** Comparison of colocalization between *KCNMA1* mRNA and mRNA from *CACNA1D*, *GAPDH*, and scrambled images of *CACNA1D*. Data points are from n = 67 cells. Scale bar is 10 µm and 1 µm in the magnifications.

synthesized proteins remain together during trafficking through the ER and the Golgi.

As an additional control, we tested the proximity between mRNAs of *KCNMA1* and voltage-gated sodium channels *SCN9A*. This sodium channel is expressed in INS-1 cells; however, we do not expect these two mRNAs to translate nearby, as these proteins do not couple functionally. We detected *SCN9A* mRNA in the same cells where *KCNMA1* mRNA was found (Figure 6A). The colocalization between *KCNMA1* mRNA and *SCN9A* mRNA was only 18 ± 2% (Figure 6C), which was less than what was observed with *KCNMA1* mRNA and *CACNA1D* mRNA (60%, Figure 5F). This result shows that *KCNMA1* mRNA tends to localize closer to *CACNA1D* mRNA than to *SCN9A* mRNA or *GAPDH* mRNA, suggesting a preference for translating nearby.

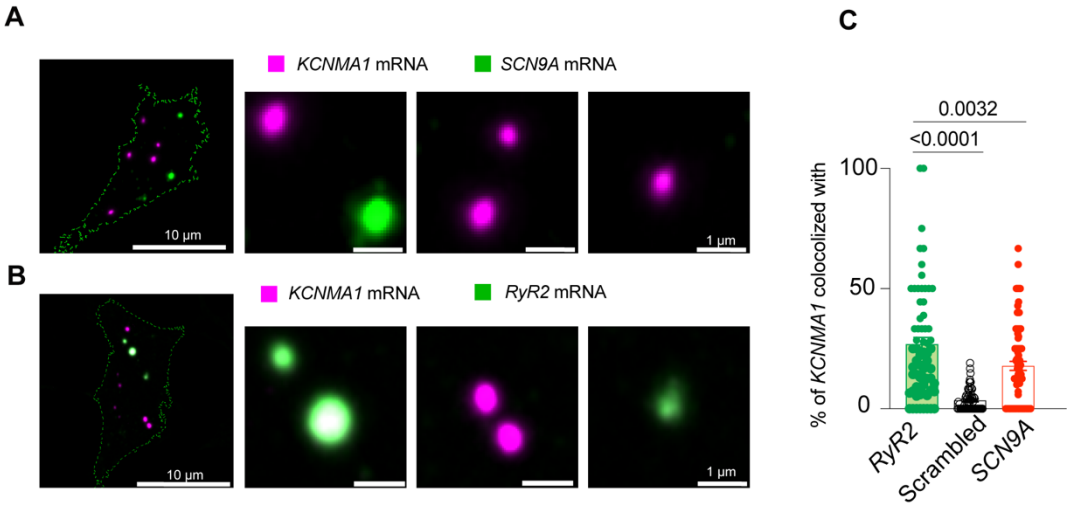

Figure 6. BK (*KCNMA1*) and RyR-2 (*RyR2*) mRNA co-localize. A. Representative confocal images of *KCNMA1* and Na$_V$1.7 (*SCN9A*) mRNA. **B.** Representative images of *KCNMA1* and *RyR2* mRNA. **C**. Comparison of the colocalization between *KCNMA1* mRNA and mRNA from *RyR2*, *SCN9A*, and scrambled images of *KCNMA1*. Data points are from n =67 cells. One way ANOVA. Scale bar is 10 µm and 1 µm in the magnifications.

With the goal of understanding if this concept could apply to other channels, we used the same approach to test a second protein known to provide calcium for BK channel opening. Similar to the coupling between BK and Ca$_V$1.3 channels, RyR2 also can be structurally coupled to BK channels [29]. Figure 5B shows high-resolution images of single-molecule in-situ hybridization for *RyR2* probed together with *KCNMA1* in INS-1 cells. In the same population of cells, *KCNMA1* mRNA and *RyR2* colocalization was 27 ± 3%, which is 1.5 times that with *SCN9A* mRNA. We also assessed *RyR2* colocalization with randomized, computer-generated *KCNMA1* mRNA signals. We found that colocalization between randomized *KCNMA1* mRNA and genuine *RyR2* mRNA was 87% less colocalized compared to the analysis of genuine *KCNMA1* mRNA and genuine *RyR2* mRNA (Figure 6C), suggesting that *KCNMA1* mRNA not only colocalizes with *CACNA1D* but also with mRNA of other known calcium sources.

Formation of BK and Ca$_V$1.3 ensembles in INS-1 cells.

We previously showed the organization of BK and Ca$_V$1.3 channels in ensembles in tsA-201 cells and neurons, including hippocampal and sympathetic motor neurons [16]. Our present study utilized INS-1 cells. We detected single molecules from BK and Ca$_V$1.3 channels in INS-1 cells using super-resolution microscopy and determined their degree of co-localization. Figure 7A shows a

representative image of the localizations of antibodies against BK and Ca$_V$1.3 channels. Maps were rendered at 5 nm, the pixel size for the images presented. BK-positive pixels formed multi-pixel aggregates, which has been interpreted as clusters of BK channels. The same was true for Ca$_V$1.3 channels. When looking at the spatial relation between BK and Ca$_V$1.3 channels, no fixed geometry or stoichiometry was observed. On the contrary, maps showed a distribution of distances between BK and Ca$_V$1.3 detected pixels. In some cases, BK and Ca$_V$1.3 channels were perfectly overlapping, as if the detection of the antibodies could not be separated by the 20 nm resolution, suggesting that the same channel aggregate contained BK and Ca$_V$1.3 channels. In other cases, BK and Ca$_V$1.3 channels were adjacent (less than 5 nm), and in other

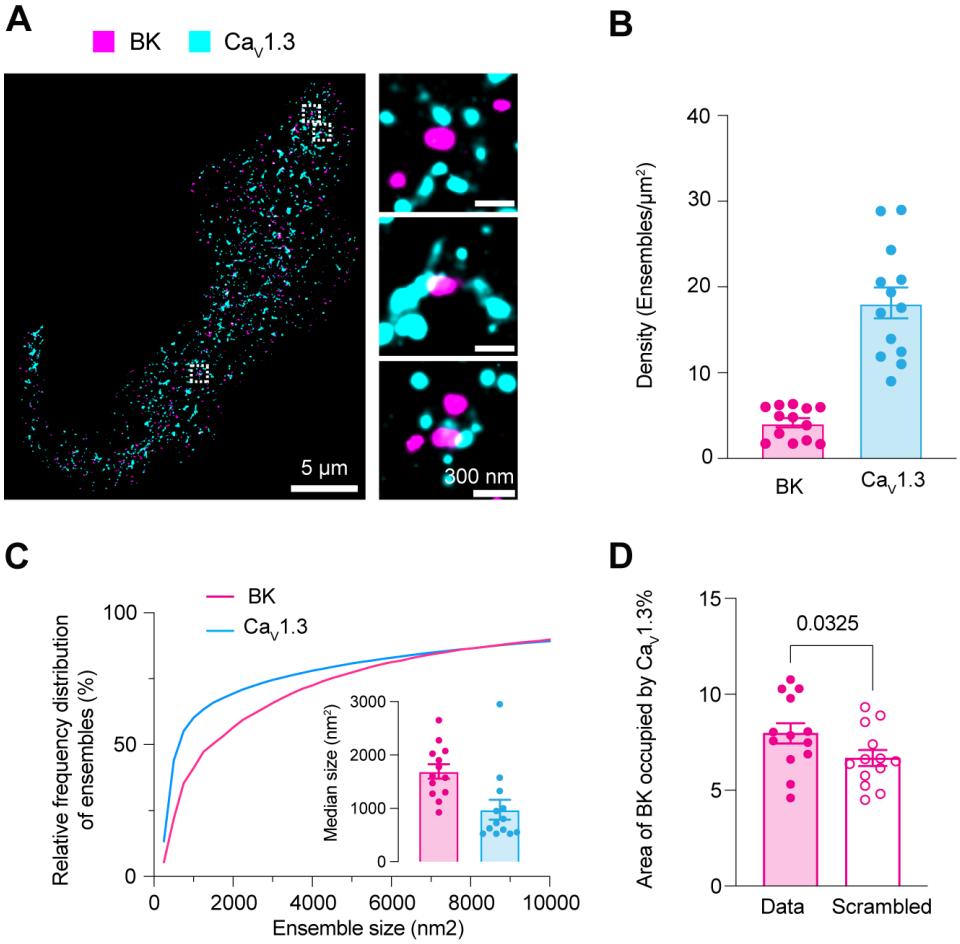

Figure 7. Formation of BK and Ca$_V$1.3 ensembles in INS-1 cells. (A) Representative localization map of antibodies against BK (magenta) or Ca$_V$ (cyan) channels. Magnifications are shown in the insets on the right. (B) Scatter dot plot of channel density of BK and Ca$_V$1.3 channels in INS-1 cells. (C) Cumulative frequency distribution of the size of BK and Ca$_V$1.3 channels. Inset compares median size of BK and Ca$_V$ channels. (D) Comparison of colocalization between BK and Ca$_V$1.3 and BK and scrambled BK images. Data points are from n = 13 cells. Scale bar is 5 µm and 300 nm in the magnifications.

cases, BK clusters were surrounded by a variable number of Ca_V1.3 channels.

To provide a more quantitative description of the maps, we measured cluster density, cluster size, and colocalization. We used the particle-analysis tool of the software ImageJ for these measurements. In this analysis, a particle represents positive pixels irrespective of the number of pixels composed. As a note, a particle of one pixel would likely to be a single channel, whereas a particle composed of many pixels would likely to be a cluster of channels. INS-1 cells showed 4 times as many Ca_V1.3 particles as BK particles (Figure 7B). Figure 6C shows the frequency distribution of particle size, where the median area is 1691 nm^2 for BK and 975 nm^2 for Ca_V1.3. We also found 7.5% colocalization between BK and Ca_V1.3 particles (Figure 7D), which was higher than the colocalization calculated using scrambled images.

Ensembles of BK and Ca_V1.3 channels are detected at the plasma membrane soon after their expression begins

In light of our results, our current model is that BK and Ca_V1.3 ensembles form prior to their insertion into the plasma membrane. One prediction based on this model is that channels inserted in the plasma membrane would appear as ensembles already at early time points after the start of their synthesis. To test this prediction, we transfected tsA-201 cells with BK and Ca_V1.3 channels and performed a chase experiment to detect their presence at the plasma membrane using super-resolution microscopy. We measured particle size, density, and colocalization 18, 24, and 48 hours after transfection. Notably, although the channels were transfected simultaneously, BK particles were detected in the plasma membrane 18 hours after transfection, whereas Ca_V1.3 particles were detected only 24 hours after transfection (Figure 8A-C). The distribution of BK and Ca_V1.3 particle size did not change with the time after transfection (Figure 8D and E), in agreement with Sato et al., 2019 [24].

In support of our prediction, we found particles of Ca_V1.3 near BK particles as soon as the expression of Ca_V1.3 channels was detected in the plasma membrane (24 hours after transfection, Enlarged Figure 8B). To test this hypothesis further, we compared plots of localization preference at 24 and 48 hours. These plots were constructed by measuring the percentage of Ca_V1.3 area occupying concentric regions of 20 nm width around BK particles. Values were normalized to the percentage of colocalization found at 200 nm from BK. Figure 8F shows that the localization preference plots are identical at

Figure 8. BK and Ca$_V$1.3 channels colocalize soon after insertion into the plasma membrane.

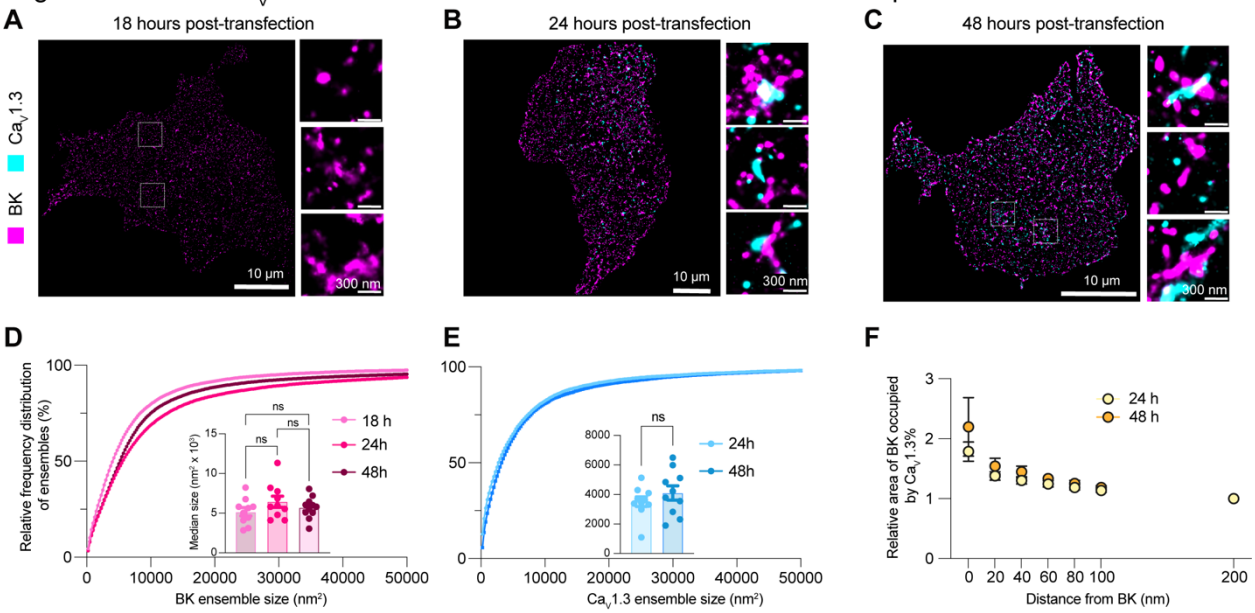

Figure 8. Ensembles of BK and Ca$_V$1.3 channels are detected at the plasma membrane soon after their expression begins. (A-C) Representative localization maps of antibodies against BK and Ca$_V$ channels (A) 18 hours, (B) 24 hours, or (C) 48 hours after DNA transfection into the cell. Enlargements are shown in insets. (D) Size distribution of BK clusters at 18, 24, and 48 hours. Inset compares median BK cluster areas. (E) Size distribution of Ca$_V$ clusters at 24 and 48-hour time points. Inset compares median Ca$_V$ cluster areas. Ca$_V$1.3 clusters are not present at the 18-hour time point. (F) Comparison of colocalization plots between BK and Ca$_V$1.3 channels at 24 and 48-hour time points. Data points are from n = 10 cells. Scale bar is 10 µm and 300 nm in enlargements.

24 and 48 hours, consistent with the idea that these channels are inserted together already as ensembles.

Discussion

Intracellular Assembly of BK and Ca$_V$1.3 Channels

Previous work from our group has revealed the organization as ensembles of large-conductance calcium-activated potassium (BK) channels and voltage-gated calcium channels, particularly Ca$_V$1.3, within nanodomains. This spatial organization is crucial for the functional coupling that enables BK channels to respond promptly to calcium influx, thereby modulating cellular excitability [15]. While physical details of BK-Ca$_V$ interactions are not fully elucidated, the evidence suggests that BK channels interact with both the Ca$_V$ α1 subunit and its auxiliary subunits [30, 31]. Our findings suggest that the co-assembly of BK and Ca$_V$1.3 channels into ensembles occurs early in the process of protein synthesis, before arrival at the Golgi. Thus, the channels would be properly configured for immediate functional interaction upon reaching the cell surface.

A stochastic model of ion channel cluster formation in the plasma membrane proposes that random yet probabilistic interactions between ion channels contribute to the formation of homo-clusters [24]. These clusters are stabilized and organized within specific membrane regions through biophysical mechanisms such as membrane curvature. Recent findings on spatial organization of G-protein coupled receptors provide additional support for this framework, demonstrating that the coupling of membrane proteins to the curvature of the plasma membrane acts as a driving force for their clustering into functional domains [32]. Yet, the mechanisms regulating the spatial organization of hetero-clusters (ensembles) are less known.

The co-localization of BK and Ca_V1.3 channels before reaching to Golgi (ER and at ER exit sites) indicates a coordinated trafficking mechanism. This coordination likely facilitates the formation of multi-channel complexes that are essential for precise calcium signaling and membrane excitability. Additionally, the presence of these ensembles in the Golgi suggests that post-translational modifications and further assembly processes occur before the channels are transported to the plasma membrane. The intracellular assembly of BK and Ca_V1.3 channels underscores the importance in ensuring efficient functional coupling, which is essential for various physiological processes, including the modulation of neurotransmission and control of neuronal firing pattern [33, 34].

mRNA Co-localization and Protein Trafficking

The co-localization of mRNAs encoding BK and Ca_V1.3 channels suggests a coordinated translation mechanism that facilitates their proximal synthesis and subsequent assembly into functional complexes. As a mechanism, mRNA localization enhances protein enrichment at functional sites, coordinating with translational control to position ion channels at specific subcellular domains, particularly critical in neurons and cardiomyocytes [35, 36]. By synthesizing these channels in close proximity, this process aids their efficient assembly into functional units reaching their target destination which is crucial for the precise targeting and trafficking of ion channels to specific subcellular domains, thereby ensuring proper cellular function and efficient signal transduction [35, 37-39]. Disruption in mRNA localization or protein trafficking can lead to ion channel mislocalization, resulting in altered cellular function and contributing to disease states. In cardiac cells, precise trafficking of ion channels to specific membrane subdomains is crucial for maintaining normal electrical and mechanical functions, and its disruption

contributes to heart disease and arrhythmias [40-42] Similarly, in neurons, the localization and translation of mRNA at synaptic sites are essential for synaptic plasticity, and disturbances can lead to neurological disorders [43, 44].

Co-translational Regulation and Functional Coordination

The co-translational association of transcripts encoding BK and Ca_V1.3 ion channels, as well as other known Ca^{2+} sources like RyR2, may serve as a mechanism to ensure the precise stoichiometry and assembly of functional channel complexes. This precise assembly is also critical for spatially organizing RyR2 and BK channels, as shown in airway myocytes, where the proximity of these channels underlies the efficient activation of BK channels by localized Ca^{2+} sparks [45]. Co-translational association of transcripts encoding K_V1.3 channels was the first example in which the interaction of nascent K_V1.3 N-termini facilitates proper tertiary and quaternary structure required for oligomerization [46, 47]. Similarly, co-translational heteromeric association of hERG1a and hERG1b subunits ensures that cardiac IK_r currents exhibit the appropriate biophysical properties and magnitude necessary for normal ventricular action potential shaping [39]. The precise mechanism by which BK transcripts are associated with the transcripts of Ca^{2+} sources like Ca_V1.3 and RyR2 channels remain to be elucidated. While it is conceivable that complementary base pairing or tertiary structural interactions play a role, RNA binding proteins (RBPs) are likely key mediators of these associations.

Conclusion and Future Directions

This study provides novel insights into the organization of BK and Ca_V1.3 channels in ensembles, highlighting the importance of their assembly within the ER, ER exit sites, and Golgi. Our findings reveal that these channels not only assemble at the plasma membrane but also form significant signaling complexes at intracellular membranes, supporting the idea of their coordinated synthesis and trafficking. These observations underscore the critical role of spatial organization in maintaining cellular excitability and calcium signaling. While our study advances the understanding of assembly of BK and Ca_V1.3 complexes, several key questions remain unanswered. What molecular machinery drives this co-localization at the mRNA and protein level? How do disruptions to complex assembly contribute to channelopathies and related diseases? Additionally, a deeper investigation into the role of RNA binding proteins in facilitating transcript association and localized translation is warranted.

Acknowledgments

We thank Gail Robertson for her immense support and influence in designing and conducting this project. We thank Alexey Merz for his support and feedback through this project. We thank Bertil Hille for his contribution to editing the writing of this project. We thank Martina Hunt, Maria Danoviz, Paula Martinez-Feduchi, Wendy Piñon-Teal, and Raul Riquelme for reading and providing feedback on the manuscript. We thank William Catterall and Ruth E. Westenbroek for providing the antibody against CaV1.3. This study was supported by the National Institutes of Health MIRA R35 GM142690 to O.V. CM was supported by HL162609 and the Freeman Hrabowski HHMI Scholars program.

Supplementary figures

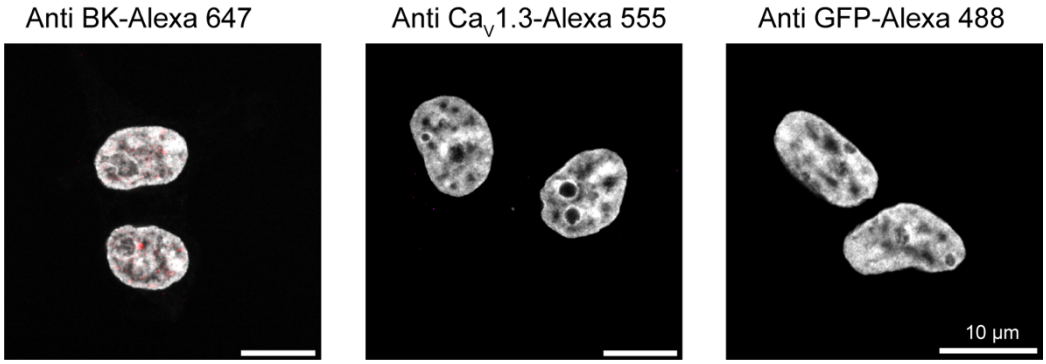

Figure 2-Supplementary 1. Validation of antibodies against BK, Ca_V1.3 and GFP. Representative confocal images of tsA-201 cells immuno-tested for BK channels (left), Ca_V1.3 channels (middle), and GFP proteins (right). Cells were not transfected. Nuclei were stained with DAPI and pseudo colored in gray. Scale bar is 10 µm for all images.

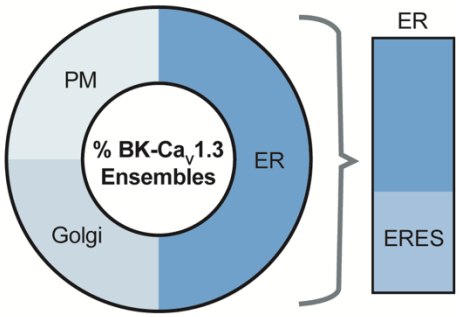

Figure 4-Supplementary 1. Diagram illustrating our interpretation of the percentage of BK-Ca_V1.3 ensembles found in the cell. This illustration is based on experiments shown in figures 1 to 4, but percentages were modified to represent overlap of fluorescent signals and limited resolution. We also show that the ensembles found in the ER exit sites (ERES) are also accounted in the ER.

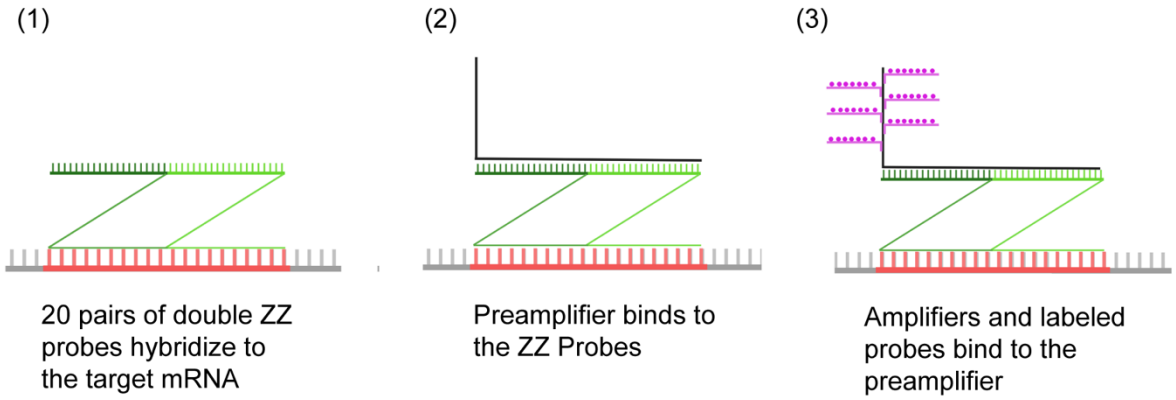

Figure 5-Supplementary 1. Illustration of RNA scope methodology. Steps to detect an mRNA sequence (red zipper) consisting of (1) hybridization, (2) pre-amplification, (3) and labeling. Double ZZ probes are shown in green. Dye labeling the mRNA is shown in magenta.

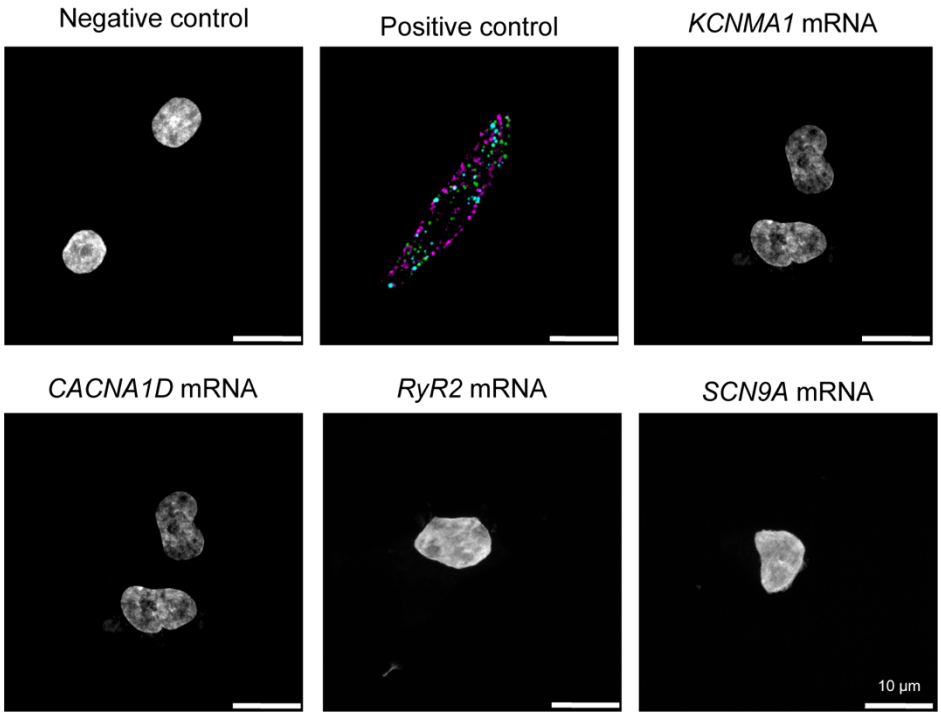

Figure 5-Supplementary 2. RNA probe validation. A. Representative images of INS-1 cells subjected to mRNA probes against a bacterial gene (DapB from *Bacillus subtilis*). **B.** Representative images of INS-1 cells subjected to mRNA probes against three constitutive mammalian genes (ubiquitin C, cyclophilin B, and a polymerase II subunit). **C - F** show tsA-201 cells that were naive to exogenous DNA but treated with mRNA probes against the genes for (**C**) BK channels, (**D**) Ca$_V$1.3 channels, (**E**) Ryanodine Receptors type 2 (RyR2), and (**F**) NaV1.7 channels. Scale bar is 10 µm.

References:

1. Contreras, G.F., et al., *A BK (Slo1) channel journey from molecule to physiology*. Channels (Austin), 2013. **7**(6): p. 442-58.
2. Kaczorowski, G.J., et al., *High-conductance calcium-activated potassium channels; structure, pharmacology, and function*. J Bioenerg Biomembr, 1996. **28**(3): p. 255-67.
3. Contet, C., et al., *BK Channels in the Central Nervous System*. Int Rev Neurobiol, 2016. **128**: p. 281-342.
4. Ancatén-González, C., et al., *Ca2+- and Voltage-Activated K+ (BK) Channels in the Nervous System: One Gene, a Myriad of Physiological Functions*. Int J Mol Sci, 2023. **24**(4).
5. Dopico, A.M., A.N. Bukiya, and J.H. Jaggar, *Calcium- and voltage-gated BK channels in vascular smooth muscle*. Pflugers Arch, 2018. **470**(9): p. 1271-1289.
6. Hu, S.L., H.S. Kim, and A.Y. Jeng, *Dual action of endothelin-1 on the Ca2(+)-activated K+ channel in smooth muscle cells of porcine coronary artery*. Eur J Pharmacol, 1991. **194**(1): p. 31-6.
7. Semenov, I., et al., *BK channel beta1-subunit regulation of calcium handling and constriction in tracheal smooth muscle*. Am J Physiol Lung Cell Mol Physiol, 2006. **291**(4): p. L802-10.
8. Dupont, C., et al., *BK channels promote action potential repolarization in skeletal muscle but contribute little to myotonia*. Pflugers Arch, 2024. **476**(11): p. 1693-1702.
9. Pallotta, B.S., K.L. Magleby, and J.N. Barrett, *Single channel recordings of Ca2+-activated K+ currents in rat muscle cell culture*. Nature, 1981. **293**(5832): p. 471-4.
10. Meredith, A.L., *BK Channelopathies andand KCNMA1-Linked Disease Models*. Annu Rev Physiol, 2024. **86**: p. 277-300.
11. Bailey, C.S., et al., *KCNMA1-linked channelopathy*. J Gen Physiol, 2019. **151**(10): p. 1173-1189.
12. Houamed, K.M., I.R. Sweet, and L.S. Satin, *BK channels mediate a novel ionic mechanism that regulates glucose-dependent electrical activity and insulin secretion in mouse pancreatic beta-cells*. J Physiol, 2010. **588**(Pt 18): p. 3511-23.
13. Shah, K.R., X. Guan, and J. Yan, *Structural and Functional Coupling of Calcium-Activated BK Channels and Calcium-Permeable Channels Within Nanodomain Signaling Complexes*. Front Physiol, 2021. **12**: p. 796540.
14. Berkefeld, H., et al., *BKCa-Cav channel complexes mediate rapid and localized Ca2+-activated K+ signaling*. Science, 2006. **314**(5799): p. 615-20.
15. Vivas, O., et al., *Proximal clustering between BK and CaV1.3 channels promotes functional coupling and BK channel activation at low voltage*. Elife, 2017. **6**.
16. Prakriya, M. and C.J. Lingle, *Activation of BK channels in rat chromaffin cells requires summation of Ca(2+) influx from multiple Ca(2+) channels*. J Neurophysiol, 2000. **84**(3): p. 1123-35.
17. Lipscombe, D., T.D. Helton, and W. Xu, *L-type calcium channels: the low down*. J Neurophysiol, 2004. **92**(5): p. 2633-41.

18. Eichel, C.A., et al., *A microtranslatome coordinately regulates sodium and potassium currents in the human heart*. Elife, 2019. **8**.
19. Liu, F., et al., *Cotranslational association of mRNA encoding subunits of heteromeric ion channels*. Proc Natl Acad Sci U S A, 2016. **113**(17): p. 4859-64.
20. Lu, J., et al., *T1-T1 interactions occur in ER membranes while nascent Kv peptides are still attached to ribosomes*. Biochemistry, 2001. **40**(37): p. 10934-46.
21. Yang, S., et al., *Membrane curvature governs the distribution of Piezo1 in live cells*. Nat Commun, 2022. **13**(1): p. 7467.
22. Chen, Z., et al., *EMC chaperone-CaV structure reveals an ion channel assembly intermediate*. Nature, 2023. **619**(7969): p. 410-419.
23. Cheng, E.P., et al., *Restoration of normal L-type Ca2+ channel function during Timothy syndrome by ablation of an anchoring protein*. Circ Res, 2011. **109**(3): p. 255-61.
24. Sato, D., et al., *A stochastic model of ion channel cluster formation in the plasma membrane*. J Gen Physiol, 2019. **151**(9): p. 1116-1134.
25. Hell, J.W., et al., *Identification and differential subcellular localization of the neuronal class C and class D L-type calcium channel alpha 1 subunits*. J Cell Biol, 1993. **123**(4): p. 949-62.
26. Costantini, L.M., et al., *A palette of fluorescent proteins optimized for diverse cellular environments*. Nat Commun, 2015. **6**: p. 7670.
27. Georgiades, P., et al., *The flexibility and dynamics of the tubules in the endoplasmic reticulum*. Sci Rep, 2017. **7**(1): p. 16474.
28. Nixon-Abell, J., et al., *Increased spatiotemporal resolution reveals highly dynamic dense tubular matrices in the peripheral ER*. Science, 2016. **354**(6311).
29. Bashour, A.M. and G.S. Bloom, *58K, a microtubule-binding Golgi protein, is a formiminotransferase cyclodeaminase*. J Biol Chem, 1998. **273**(31): p. 19612-7.
30. Rehak, R., et al., *Low voltage activation of KCa1.1 current by Cav3-KCa1.1 complexes*. PLoS One, 2013. **8**(4): p. e61844.
31. Zhang, F.X., et al., *BK Potassium Channels Suppress Cavα2δ Subunit Function to Reduce Inflammatory and Neuropathic Pain*. Cell Rep, 2018. **22**(8): p. 1956-1964.
32. Kockelkoren, G., et al., *Molecular mechanism of GPCR spatial organization at the plasma membrane*. Nat Chem Biol, 2024. **20**(2): p. 142-150.
33. Berkefeld, H., B. Fakler, and U. Schulte, *Ca2+-activated K+ channels: from protein complexes to function*. Physiol Rev, 2010. **90**(4): p. 1437-59.
34. Loane, D.J., P.A. Lima, and N.V. Marrion, *Co-assembly of N-type Ca2+ and BK channels underlies functional coupling in rat brain*. J Cell Sci, 2007. **120**(Pt 6): p. 985-95.
35. Vacher, H., D.P. Mohapatra, and J.S. Trimmer, *Localization and targeting of voltage-dependent ion channels in mammalian central neurons*. Physiol Rev, 2008. **88**(4): p. 1407-47.
36. Medioni, C., K. Mowry, and F. Besse, *Principles and roles of mRNA localization in animal development*. Development, 2012. **139**(18): p. 3263-76.
37. Blandin, C.E., et al., *Remodeling of Ion Channel Trafficking and Cardiac Arrhythmias*. Cells, 2021. **10**(9).

38. Dai, G., *Signaling by Ion Channels: Pathways, Dynamics and Channelopathies*. Mo Med, 2023. **120**(5): p. 367-373.
39. Jameson, M.B., et al., *Pairwise biosynthesis of ion channels stabilizes excitability and mitigates arrhythmias*. Proc Natl Acad Sci U S A, 2023. **120**(42): p. e2305295120.
40. Anderson, C.L., et al., *Most LQT2 mutations reduce Kv11.1 (hERG) current by a class 2 (trafficking-deficient) mechanism*. Circulation, 2006. **113**(3): p. 365-73.
41. Smyth, J.W. and R.M. Shaw, *Forward trafficking of ion channels: what the clinician needs to know*. Heart Rhythm, 2010. **7**(8): p. 1135-40.
42. Basheer, W.A. and R.M. Shaw, *Connexin 43 and CaV1.2 Ion Channel Trafficking in Healthy and Diseased Myocardium*. Circ Arrhythm Electrophysiol, 2016. **9**(6): p. e001357.
43. Eliscovich, C., S.M. Shenoy, and R.H. Singer, *Imaging mRNA and protein interactions within neurons*. Proc Natl Acad Sci U S A, 2017. **114**(10): p. E1875-E1884.
44. Yoon, Y.J., et al., *Glutamate-induced RNA localization and translation in neurons*. Proc Natl Acad Sci U S A, 2016. **113**(44): p. E6877-E6886.
45. Lifshitz, L.M., et al., *Spatial organization of RYRs and BK channels underlying the activation of STOCs by Ca(2+) sparks in airway myocytes*. J Gen Physiol, 2011. **138**(2): p. 195-209.
46. Robinson, J.M. and C. Deutsch, *Coupled tertiary folding and oligomerization of the T1 domain of Kv channels*. Neuron, 2005. **45**(2): p. 223-32.
47. Tu, L. and C. Deutsch, *Evidence for dimerization of dimers in K+ channel assembly*. Biophys J, 1999. **76**(4): p. 2004-17.